Extreme Anomalous Conductance Enhancement in Neutral Diradical Acene-like Molecular Junctions

Brent Lawson[1], Efrain Vidal Jr.[2,3], Sigifredo Luna[4], Michael M. Haley*[,2,3] and Maria Kamenetska*[,1,4,5]

[1]Department of Physics, Boston University, Boston, MA, USA
[2]Department of Chemistry & Biochemistry, University of Oregon, Eugene, OR, USA
[3]Materials Science Institute, University of Oregon, Eugene, OR, USA
[4]Department of Chemistry, Boston University, Boston, MA, USA
[5]Division of Material Science and Engineering, Boston University, Boston, MA, USA
e-mail: mkamenet@bu.edu; haley@uoregon.edu

Abstract:

We achieve, at room temperature, conductance enhancements over two orders of magnitude in single molecule circuits formed with polycyclic benzoquinoidal (**BQ$_n$**) diradicals upon increasing molecular length by ~5 Å. We find that this extreme and atypical anti-ohmic conductance enhancement at longer molecular lengths is due to the diradical character of the molecules, which can be described as a topologically non-trivial electronic state, and results in constructive interference between the frontier molecular orbitals. The unique feature of the compounds studied here as molecular wires is that they are characterized by high diradical character in the neutral state, allowing for robust and facile measurements of their transport properties. We adapt the 1D-SSH model, originally developed to examine electronic topological order in linear carbon chains, to the polycyclic systems studied here and find that it captures the anti-ohmic trends in this molecular series. Specifically, our model reveals that the mechanism of conductance enhancement with length in polycyclic systems is constructive quantum interference (CQI) between the frontier orbitals with non-trivial topology, which is present in acene-like, but not in linear, molecular

systems. Importantly, we use our model to predict and experimentally validate that anti-ohmic trends can be engineered through synthetic adjustments of the diradical character of the acene-like molecules. Overall, we achieve an experimentally unprecedented anti-ohmic enhancement and mechanistic insight into electronic transport in a class of materials that we identify here as promising candidates for creating highly conductive and tunable nanoscale wires.

Introduction

With increasing drive for miniaturization, the properties of nanoscale materials such as individual particles or molecules take on added significance for the development of future technologies. For example, passing electronic current across single molecules attached to metal electrodes has been shown to result in switching or diode-like behavior, raising the prospect of molecules as active components in next generation electronic devices.[1–5] Appealingly, the properties of such molecular circuits can be tuned using synthetic control of the molecular atomic structure. A challenge in the field is that electronic states of an organic molecular bridge are typically off-resonance with the Fermi energy of the conducting electrons in the metal.[6–9] As a result, typical molecular junctions behave as quantum tunnel barriers and tend to be highly insulating, with an electronic conductance that decreases exponentially with molecule length. Thus, with few exceptions, molecules longer than ~2 nm in length have vanishing conductance and therefore possess limited usefulness as candidates for nanoscale electronics. Developing molecular materials that overcome this limitation, known as *ohmic* decay, is an important challenge for the field.

Recent work has identified radical molecules with open-shell electronic structures containing unpaired electrons, as molecular wires with topologically non-trivial electronic states that can sustain higher conductance over longer lengths.[10–15] At room temperature and ambient conditions, charged diradicals generated through chemical oxidation were shown to exhibit *anti-ohmic* behavior, with conductance increasing modestly with molecular length up to ~2 nm and then decreasing again.[11] This reversal to typical conductance decay in longer charged organic diradicals was attributed to decreased coupling of edge topological states across the extended molecular backbone due to their localized character and the rotational degrees of freedom of phenyl constituents in the molecules.[11,16] Incorporating a chain of charged radicals in series in a single molecule restored anti-ohmic trends at longer molecular lengths, but required challenging experimental protocols to maintain the high oxidation charged state of a single organic wire.[13]

Here, we report extreme anti-ohmic behavior at room temperature in neutral diradicaloid molecules composed of cyclic benzoquinoidal units linearly fused together as in acenes, which we term the **BQ$_n$** series (Figure 1a). Unlike the aforementioned unstable, charged radical series, the neutral, stable **BQ$_n$** molecules are inherently diradicaloid. Critically, we observe that conductance is enhanced over two orders of magnitude for a molecular backbone length increase of ~5 Å from **BQ$_1$** to **BQ$_3$** even at low bias voltage. This is by far the highest enhancement observed to date and suggests at the unique potential of the neutral polycyclic diradicals to serve as efficient electron transport nanowires. These neutral systems are robust to oxidation and display increased anti-ohmic character at higher bias voltage. We measure the I-V characteristics to reveal that the HOMO-LUMO energy gap of the **BQ$_n$** series shrinks as expected with extended molecule length but, critically, that transmission does *not* decay in the HOMO-LUMO gap as it does in most other quasi-1D nanowires. We adapt and extend the 1D Su-Schrieffer-Heeger (1D-SSH) formalism to model the topological phases in cyclic planar aromatic compounds studied here and combine it with the non-equilibrium Green's function method to predict conductance trends. We demonstrate that the anti-ohmic behavior observed experimentally is intrinsic in this family of molecules when realistic bond-order parameters are incorporated into the 1D-SSH parametrization. Our analysis reveals that the conductance enhancement we observe is due to growing constructive quantum interference (CQI) between the frontier orbitals in fused cyclic systems, which we demonstrate to be a unique feature of our polycyclic system. ~~In contrast, in linear conjugated polymers like polyacetylene, destructive quantum interference (DQI) causes a drop in transmission probability in the HOMO-LUMO energy gap, resulting in near constant conductance with increasing molecular length as has been confirmed experimentally in recent studies.~~ Finally, we leverage the tunability of the molecular system to demonstrate further enhancement of anti-ohmic behavior in a related set of benzothiophene-fused quinoidal molecules (**BTQ$_n$**, Figure 1a) with higher diradical character than the **BQ$_n$** series. Overall, our study identifies a new class of 1D molecular materials as superior nanowires and provides an analytical framework and mechanistic insights needed to guide the development of highly conducting molecular circuits.

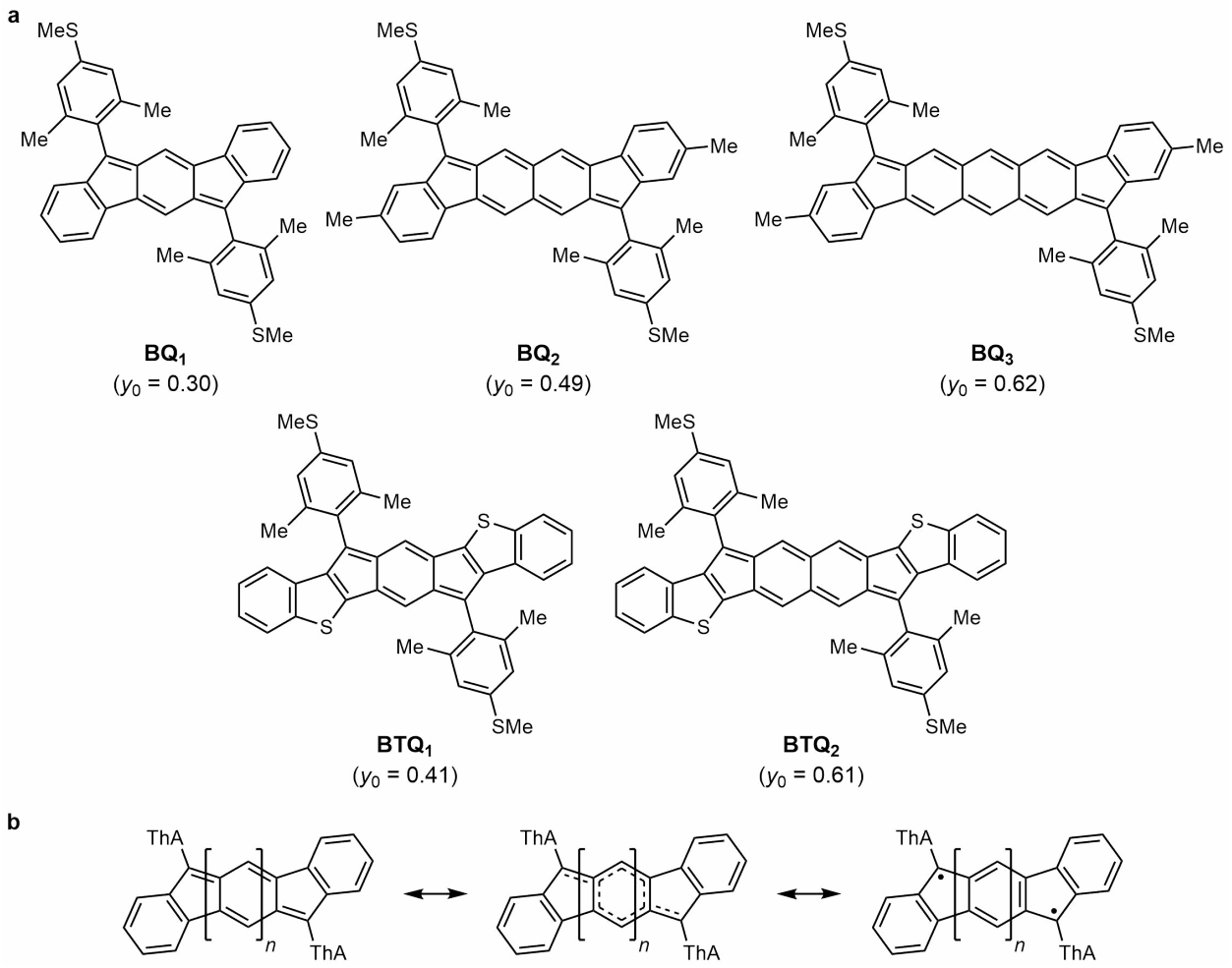

Figure 1. (a) Molecular structures of the **BQ** and **BTQ** molecules; calculated y_0 values (PUHF) are from ref. 21. (b) Resonance structures converting between the quinone, delocalized, and diradical form of the family of benzo-fused quinoids (**BQ$_n$**) where n = 1-3. Thioanisole linkers (ThA = 2,6-dimethyl-4-(methylthio)phenyl) serve to anchor the molecule to gold electrodes in the junction.

Results and Discussion

We perform room temperature single molecule conductance measurements of the **BQ$_n$** series using a scanning tunneling microscope break junction (STMBJ) technique.[17–19] The **BQ$_n$** series shown in Figure 1a are characterized by modest to intermediate diradical character, y_0, in their uncharged state.[20,21] Generally, as the number of fused six-membered rings increases, the diradical character of the molecule also increases, reflecting a higher residence of the molecules

in the diradical structure (Figure 1b, right) over the quinone (Figure 1b, left)). Overall, these molecules have been shown to be air-stable open-shell diradical singlets in the ground state, with long term stability at room temperature.[20,22–26] Importantly, the diradical character y_0, which can be tuned rationally via judicious structural modification, is inherent to the molecule and independent of solvent conditions.[23]

The **BQ$_n$** and **BTQ$_n$** were prepared analogously to their previously reported mesityl analogues via the reaction of the lithiate prepared from 4-bromo-3,5-dimethylthioanisole (ThA) with the corresponding **BQ** and **BTQ** diones. Subsequent reductive dearomatization with $SnCl_2$ afforded the target molecules; see the Supporting Information for the synthetic and spectroscopic details. Inclusion of the thioanisole functionality is critical to ensure binding to the Au electrodes. All measurements in the STMBJ were performed in 1 mM solution of 1-bromonaphthalene (BNP), a nonpolar organic solvent.

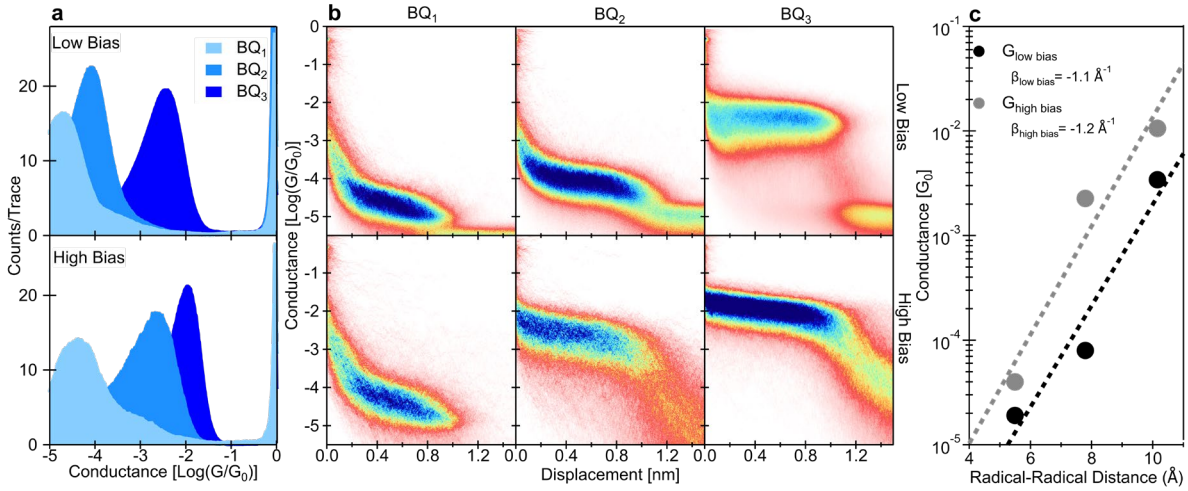

Figure 2. (a) Single-molecule conductance histograms of **BQ$_{1\text{-}3}$** in BNP at low bias, –100 mV, in the top panel and high bias, –833 mV for **BQ$_{1\text{-}2}$** and –250 mV for **BQ$_3$**, in the bottom panel. (b) Single-molecule 2D conductance vs displacement histograms of **BQ$_{1\text{-}3}$** at low bias in the top three panels and high bias in the bottom three panels. (c) Calculated conductance from Gaussian fits to the peaks in Figure 2a for both low bias (black) and high bias (gray) with exponential fits given by the dashed lines.

The 1D and 2D conductance histograms constructed from more than 5000 traces recorded in the presence of molecules **BQ1-3** are shown in Figures 2a,b. We compare conductance of the molecules measured at low bias (100 mV) and high bias (> 250 mV) on the top and bottom of the figures, respectively. In both conditions, we observe distinct conductance peaks, attributable to the formation of stable single molecule junctions with each molecule. Importantly, we observe a conductance increase with increasing molecule length from 1 to 3 repeating quinoidal units. The most likely conductance of each molecule, determined from gaussian fits to the histograms, increases over two orders of magnitude upon a molecular backbone increase of ~5Å (Figure 2c). To estimate the average rate of increase of conductance with length, we fit an exponential model to the experimental data in Figure 2c of the form:[27]

$$G = G_c e^{-\beta L}$$

where G_c is the contact conductance, β is the conductance decay constant, and L is the length of the molecules. We obtain a negative beta value of –1.1 $Å^{-1}$ for the low bias measurements. We note that the data deviate slightly from pure exponential growth as has been found previously for cationic radicals.[13] Nevertheless, the negative value of the extrapolated decay constant, $\beta < 0$, indicates a reverse conductance decay and anti-ohmic transport trends in these molecules in the absence of chemical or electric oxidation.

Measurements at high bias, 833 mV for **BQ1-2** and 250 mV for **BQ3**, show a further enhancement in single molecule junction conductance compared with measurements at 100 mV, especially for n = 2 and n = 3 (Figures 2a,b bottom). The high bias voltages correspond to the conditions that can be sustained reliably by each molecular junction over several hours of data acquisition (see Supplementary Information for more details). We also observe that the distribution of measured conductance values for **BQ3** narrows at higher bias, which has been previously identified as a signature of near-resonant transport.[28] Increases in the conductance of **BQ2-3** at

higher bias enhance the anti-ohmic characteristics, with a fit to the most likely conductance values yielding a β of –1.2 Å^{-1} (Figure 2c). This corresponds to an unprecedented increase of nearly *three orders of magnitude* in conductance from n = 1 to n = 3.

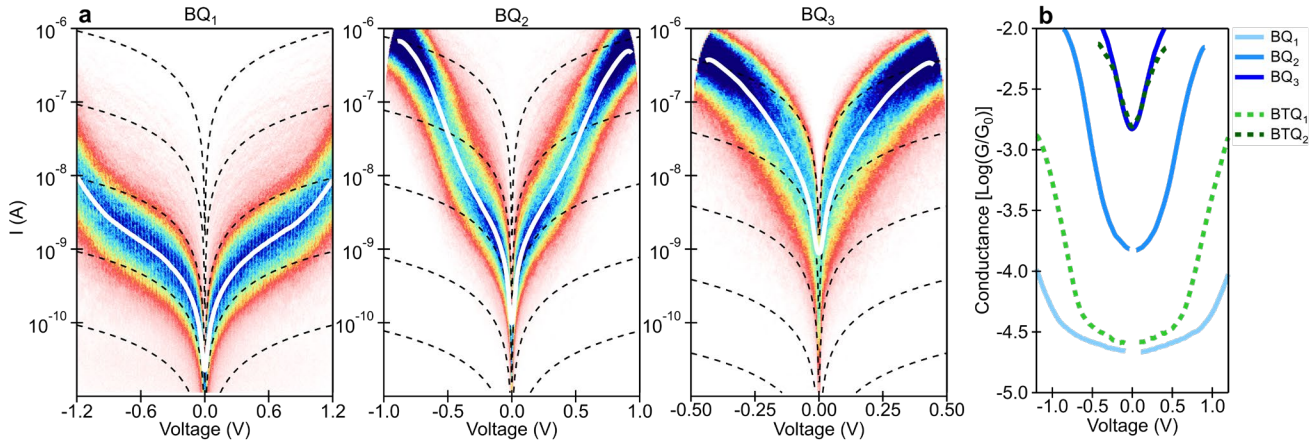

Figure 3. (a) Current-Voltage histograms for **BQ$_{1\text{-}3}$** from thousands of IV curves taken while holding each molecule between two Au electrodes. Dotted lines correspond to the linear grid lines and the white lines are calculated from the average of gaussian fits of vertical slices of each histogram IV histogram. (b) Fits of the conductance-voltage histograms derived from the current-voltage histograms for **BQ$_{1\text{-}3}$** and **BTQ$_{1\text{-}2}$**.

To understand the voltage dependent conductance behavior of each molecule and estimate the position of the frontier electron orbitals relative to E_F, we perform single molecule current-voltage (IV) measurements by sweeping the voltage between the two electrodes while the molecule is held in the junction and recording the current using previously published protocols; additional details are provided in the Supplementary Information.[29] IV histograms for **BQ$_{1\text{-}3}$** (Figure 3a) are constructed from at least 5000 traces with the average IV curve, shown in white, calculated from gaussian fits to vertical slices at each voltage. The dashed black lines are linear curves shown for references. We observe that in all three cases, the molecular IV characteristics are non-linear at a range of biases probed here. For the shortest molecule, a linear current-voltage relationship is observed below ~500mV, but the current starts to increase exponentially above ~600 mV,

suggesting that at this higher bias, the probed voltage range of ± 300 mV around E_F approaches a resonance feature associated with a frontier electronic state in the transmission spectrum of **BQ_1**. In the longer molecules, **BQ_2** and **BQ_3**, the exponential increase sets in above 100 and 0 mV, respectively, indicating the presence of molecular resonances within narrower voltage ranges for the longer molecules. Overall, the IV curves for the three molecules indicate a decreasing distance to one of the frontier orbitals as the number of repeating fused benzene units increases, suggesting a smaller HOMO-LUMO energy gap, E_{gap}, in longer molecules.

We replot the averaged IV curves from Figure 3a as conductance and group them for direct comparison in Figure 3b. The sharp upturns in these conductance spectra correspond to the supra-linear regions of the IV curves noted above. Importantly, we observe that the conductance at low bias, which probes transport in the vicinity of the E_{gap} midpoint, follows anti-ohmic behavior. This reverse, anti-ohmic conductance decay at all bias regimes is anomalous compared to transport trends through most single molecule junctions observed to date. The data confirms that the neutral acene-like materials display anti-ohmic behavior in their neutral state, even in mild and accessible experimental conditions.

We develop a 1D-SSH model appropriate for describing the contribution of the diradical character to the electron transport properties of quinonic molecular systems, such as BQ_n studied here in order to probe the mechanism behind anti-ohmic transport. In prior studies, the 1D-SSH, or tight-binding, Hamiltonian was used to describe electronic phases in linear chains such as polyenes or polymethine, which are molecules composed of a series of alternating single and double bonds, as shown in the purple path through BQ_1 (Figure 4a).[16,30] In a Hamiltonian formalism, the double and single bonds correspond to a large and small coupling energy respectively.[7] For linear molecules, a single parameter δ was used to parameterize the transition between resonance structures, with $1 > \delta > -1$, spanning the range from zero diradical character $y_0 = 0$, to full diradical, $y_0 = 1$, respectively. For this parameterization, the coupling energy terms t_1

and t_2 are set to scale as $t_0 e^{\pm a\delta}$, with t_0 and a set to 1, resulting in the purple bonds alternating between double (high coupling) and single (low coupling) as δ goes between –1 ($t_1 < t_2$ → diradical) and 1 ($t_1 > t_2$ → polyene).[7,16] Intermediate values of δ describe intermediate scenarios, with δ = 0 corresponding to a delocalized electronic state with 50% diradical character. As fully diradical polyenes (δ=-1) are not stable and thus experimentally inaccessible, this earlier model can instead be applied to cumulenes or polymethines, which are linear carbon chains with a fully delocalized state well approximated by the δ = 0. In cumulenes and other molecular chains, conductance was found to remain nearly constant as the molecular length increased.[16,31–33]

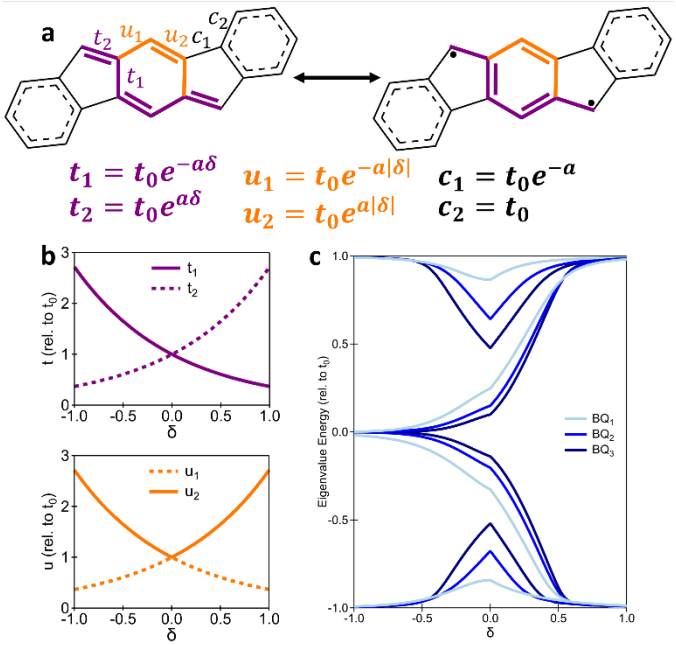

Figure 4. Modification to the 1D-SSH Model for polycyclic molecular systems like **BQ_n**. (a) Description of the coupling energies (t_0, t_1, t_2, u_1, u_2, c_1, c_2) describe by diradical parameter (δ) and scaling parameter (a) used in the modified 1D SSH Hamiltonian. (b) Graphical representation of the energies t_1, t_2, u_1, u_2. (c) The calculated band structure for **$BQ_{1\text{-}3}$** as a function of δ.

Here, we implement a modified 1D-SSH Hamiltonian for polycyclic systems. We include an additional set of hopping parameters, u_1 and u_2, shown in orange (Figure 4a), which are not

entirely independent from t_1 and t_2. For example, unlike the purple bonds, the orange bonds do not flip from double to single in the transition from $\delta = -1$ (diradical aromatic) to $\delta = 1$ (closed-shell quinone). Instead, these bonds are described by alternative coupling terms (u_1, u_2) given by $t_0 e^{\pm a|\delta|}$ and they retain the same bond order value at $\delta = -1$ as at $\delta = 1$ (Figure 4b). Critically, using this parameterization, all bonds t_1, t_2, u_1 and u_2 are equivalent when $\delta = 0$ and the molecule is in a fully delocalized state. The delocalized benzene ring at the extrema of the molecules are described as constants (c_1, c_2) independent of δ, in agreement with previous experimental characterization of these systems.[20,23,25]

Using this model, we calculated the eigenvalues near E_F as a function of δ (Figure 4c). As expected, the electronic structure transitions between the quinone ($\delta = 1$) and diradical ($\delta = -1$) states as the range of δ is scanned. As in the polyene system, here we observe a wide bandgap in the quinone structure, which closes as the molecule become a diradical.[34] These results confirm that our modification to the 1D-SSH model preserves the characteristic of the 1D topological insulators state at $\delta = -1$, with $E_{gap} \rightarrow 0$ in this limit.

To model transport in the **BQ$_n$** series, we convert the unitless 1D-SSH model above to a realistic energy scale characteristic of sp^2 systems containing alternating double bonds. We use established double-bond coupling energy parameters for conjugated systems and the observed bond-orders in such systems to fit t_0 and a.[7,35,36] We obtain $t_0 = 2.7eV$ and $a = 0.08$ (Supplemental Information). Establishing this realistic 1D-SSH parameterization allows for the conversion of the reported diradical character y_0 to δ as $\delta = -2y_0 + 1$. We note that the previously measured diradical character of $BQ_{1,2,3}$ correspond to $\delta = 0.4$, 0 and –0.2, respectively (Figure 5a).

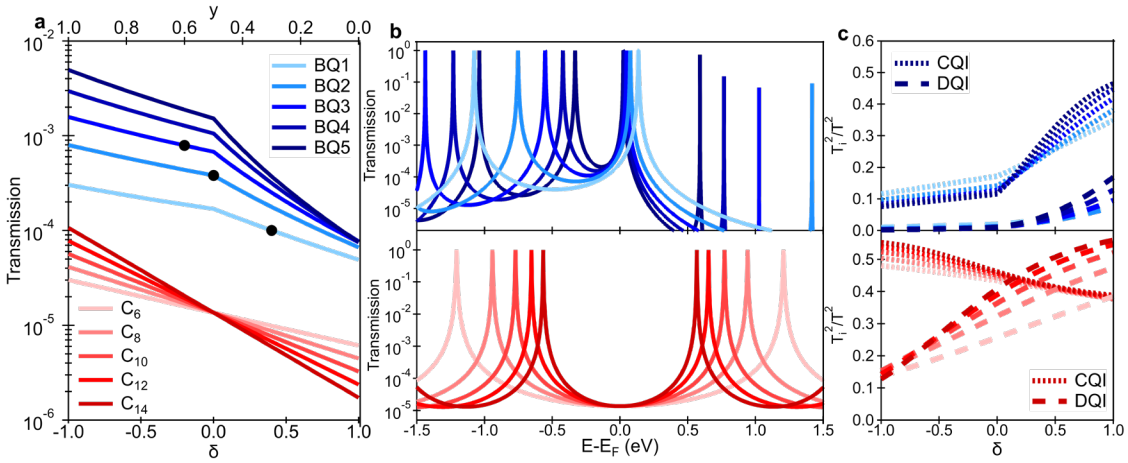

Figure 5. Unique anti-ohmic behavior of acene-like systems is due to quantum interference effects. (a) Calculated transmission at E-E_F = 0 eV of $\mathbf{BQ_n}$ series and $\mathbf{C_n}$ series as a function of diradical character. (b) Transmission curves for $\mathbf{BQ_n}$ series (top) and $\mathbf{C_n}$ series (bottom) for the case δ = 0. (c) Contribution of constructive quantum interference (CQI, dotted) and destructive quantum interference (DQI, dashed) to the total transmission for $\mathbf{BQ_n}$ and $\mathbf{C_n}$ series as a function of δ.

We use the wideband limit within the non-equilibrium Green's function (NEGF) approach described previously and in the Supplementary Information to calculate the transmission of molecules $\mathbf{BQ_n}$ as a function of δ and compare them to the standard polyene (polyacetylene) case, $\mathbf{C_n}$ (Figure 5a).[16,37,38] We calculate the polyene transmission using the standard 1D-SSH model with the realistic parameterization described above. In both cases, we observe that predicted conductance depends both on the diradical character δ and on the length of the molecular wire (Figure 5a). Importantly, however, we observe that in the case of the polycyclic quinoidal systems studied here and plotted in blue, transport is predicted to be anti-ohmic at *all* values of δ. Our model predicts that even in the closed-shell $\delta = 1$ case, molecules of different length will follow modest reversed conductance decay. We note that this expectation for closed-shell polycyclic molecules is consistent with recent observations of non-decaying conductance trends in porphyrin wires.[39,40] This prediction for polycyclic molecules is in direct contrast to the linear polyene chains, $\mathbf{C_n}$, plotted in red, where transport is predicted to decay exponentially with molecule length for $\delta > 0$ and becomes anti-ohmic only in the experimentally inaccessible regime of $\delta < 0$. These

predictions are consistent with prior work. For example, for polyenes, at $\delta = 0$, transmission in Figure 5 (bottom) is independent of length, in agreement with experimental measurements of cumulene and polymethine wires.[32,33,41,42] In contrast, for the **BQ$_n$** series, characterized by an n and δ value marked by black points in Figure 5a, the qualitative predictions of conductance enhancement match well to our experimental measurements. At the Fermi energy, the enhancement of BQ3 over BQ1 conductance predicted by the model is a factor of ~8, but at ~50 mV of bias voltage, it grows to a factor of ~100, which is in agreement with measurements at low bias in Figure 2. We note that the model does not account for electrostatic changes due to electrode shape or solvent environment, so the predicted energy alignment cannot be expected to match the experiment exactly. As the intermediate diradicals BQn have a small energy gap due to the edge state contributions, these slight variations will result in large deviations of measured conductance from predicted values. However, we note that the essential features and trends in the transmission calculated using the 1D-SSH agree well with the more computationally expensive density functional theory (DFT)-based transmission calculations of relaxed junction geometries (Figure S23), in agreement with previous theoretical calculations.[43,44] Our results suggest that the 1D-SSH one-electron model of the π system captures the experimentally observed anomalous conductance enhancement in the **BQ$_n$** series.[41]

Unlike many-body correlations, quantum interference (QI) among the frontier orbitals is included in the one-electron 1D-SSH formalism and is thus a candidate mechanism for the distinct conductance phenomena observed here in the **BQ$_n$** molecules. Previous work shows that QI effects can be explained by symmetry considerations of frontier MOs. To investigate the contribution of QI to transport trends in diradicals, we first compare the transmission spectra of polyenes and polycyclic systems at $\delta = 0$ calculated using the 1D-SSH (Figure 5b). We observe that in both series, the E_{gap} shrinks as the molecules grow longer, as expected from basic considerations of energy spacing with system size. However, for polyenes, the zero-bias conductance at E_F, remains constant, even as the band-gap closes, as was discussed above. This feature is a signature of

destructive quantum interference (DQI) between the frontier orbitals.[9] In fact, ohmic conductance decay observed in the majority of polymeric molecular wires can be attributed to DQI, which counteracts the decrease in E_{gap} at longer lengths to cause dips in transmission at E_F. In contrast, the predicted zero-bias transmission in **BQ$_n$** grows with molecule length concomitantly with the closing of the band-gap, suggesting that DQI is a less significant factor in the polycyclic diradical system.

We calculate the CQI and DQI contributions explicitly using methods reported previously using the output of the 1D-SSH model developed here (Figure 5c).[9] We observe very distinct QI trends in the linear polyene and polycyclic molecular systems. In polyenes **C$_n$**, the transition from anti-ohmic to ohmic conductance coincides with an increase in DQI and a decrease in CQI as δ goes from –1 to 1.[45] Specifically, DQI (CQI) increases (decreases) in magnitude from ~20% (~45%) to ~40% (~35%) of the total transmission. At δ=0, CQI and DQI approximately cancel. In contrast, for the **BQ$_n$** series, the CQI contribution dominates at all regimes and grows from ~20% to ~40% with increasing δ, while the DQI fraction increases slightly but remains below ~20%. These trends corroborate and explain the origin of the extreme anti-ohmic behavior observed in **BQ$_n$** compared to other polymers with diradical character. Critically, we see that in the case of polycyclic systems, increasing diradical character coincides with increasing CQI, providing mechanistic insight into engineering conducting molecular wires.

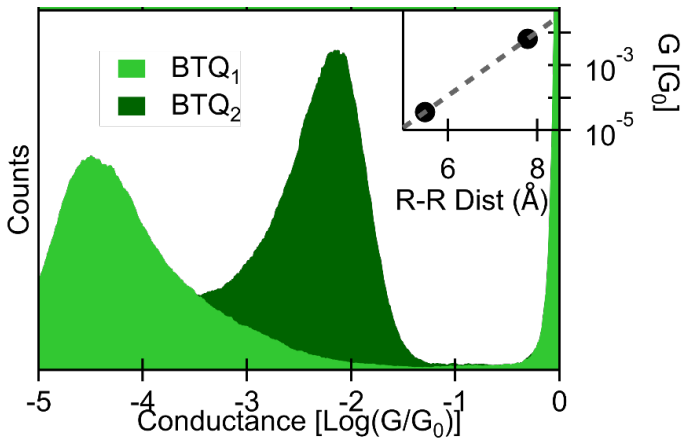

Figure 6. Engineering enhancement in anti-ohmic conductance through synthetic control. Single-molecule conductance histograms of **BTQ$_{1\text{-}2}$** (structures shown in Figure 1a) in BNP at –500 mV. Inset: most likely conductance of **BTQ$_{1\text{-}2}$** determined from the histograms plotted against radical-radical (R-R) distance results shows inverse decay and a β value of –2.3/Å.

To demonstrate the power of this experimental system, we measure the conductance of a derivative of the **BQ** series with benzothiophene elements fused to the benzoquinodal core with the thiophene S atoms in an *anti*- orientation to the diradical site (Figure 1a).[46] We term these the **BTQ$_n$** and note that the backbone length of the quinoidal cores and structure of these molecules is identical to the **BQ$_n$**. **BTQ$_n$** have been previously shown to have higher diradical character than **BQ$_n$** for the same number of fused benzoquinone units n (Figure 1a).[23] We measure the conductance of **BTQ$_n$** for n = 1, 2 at a bias V = 500 mV (Figures 6 and S25). We observe that conductance of this series is higher than in **BQ$_n$** of identical length, particularly for the longer **BTQ$_2$** molecule. The IV curves for the **BTQ$_n$** series are plotted in Figure 3b for direct comparison to **BQ$_n$**. Significantly, the conductance of **BTQ$_2$** is enhanced compared to **BQ$_2$** by at least one order of magnitude at all bias regimes, despite their identical radical-radical and overall lengths. We also note the inferred smaller E_{gap} for **BTQ$_2$** compared to **BQ$_2$** as a result of increasing diradical character. Overall, we achieve an unprecedented reverse conductance decay in the **BTQ$_n$** series, with a β value of –2.3 Å^{-1} (Figure 6 inset).

Conclusions

We have identified a unique class of molecular organic diradicals with a fused polycyclic core, where the equilibrium electronic structure is optimal for conductance enhancement at longer molecular lengths. We develop a 1D-SSH model which provides mechanistic insight into the source of conductance enhancement and identify quantum interference effects as key to anti-ohmic transport inherent to these systems. Crucially, we apply this understanding to demonstrate how molecular acene-like system can be synthetically altered and designed to further tune the diradical

character, bandgap and QI to engineer molecular junctions with higher conductance and unprecedented anti-ohmic trends. These results set the stage for future engineering of conductance enhancement and other functional behaviors in cyclic diradicals based on an acene core.

Experimental Methods

STMBJ measurements are performed by repeatedly crashing and pulling out an Au tip from an Au substrate in the presence of molecules in solution, with a fixed bias across the two electrodes while recording the current, voltage, as well as the electrode displacement. Conductance is calculated at every displacement point during pull out by dividing current by voltage to generate a conductance trace. Plateaus in the conductance trace indicate formation of persistent junction configurations with a well-defined conductance. We statistically analyze the measurements by constructing 1D conductance histograms and 2D conductance vs displacement histograms from thousands of individually recorded raw data traces as detailed previously.[19,47,48] Reproducible molecular conductance plateaus result in peaks in the histograms in the conductance range below 1 G_0.

Associated Content

Supporting Information

The Supporting Information is available free of charge at https://pubs.acs.org/doi/10.1021/xxxxxx.

Detailed synthetic procedures and full chemical characterization, UV-Vis and NMR spectra, IV measurement procedure and addition data, modified 1D SSH model, quantum interference calculations, and DFT comparisons (PDF)

Author Contributions

M.K. and M.M.H. conceived the project. E.V. synthesized and characterized the samples. B.L. performed the single molecule measurements, developed the modified 1D-SSH model and carried

out the calculations. S.L. assisted with data analysis and calculations. B.L. and M.K. wrote the paper with key contributions from E.V. and M.M.H. The manuscript reflects the contributions and ideas of all authors.

Notes

The authors declare no competing interests.

Acknowledgements

MK and BL were supported by the US National Science Foundation (CHE-2145276 to MK). The synthetic part of this study (EF and MMH) was supported by the US National Science Foundation (CHE-2246964 to MMH).

References

(1) Aviram, A.; Ratner, M. A. Molecular Rectifiers. *Chem. Phys. Lett.* **1974**, *29* (2), 277–283. https://doi.org/10.1016/0009-2614(74)85031-1.

(2) Quek, S. Y.; Kamenetska, M.; Steigerwald, M. L.; Choi, H. J.; Louie, S. G.; Hybertsen, M. S.; Neaton, J. B.; Venkataraman, L. Mechanically Controlled Binary Conductance Switching of a Single-Molecule Junction. *Nat. Nanotechnol.* **2009**, *4* (4), 230–234. https://doi.org/10.1038/nnano.2009.10.

(3) Yuan, L.; Nerngchamnong, N.; Cao, L.; Hamoudi, H.; Del Barco, E.; Roemer, M.; Sriramula, R. K.; Thompson, D.; Nijhuis, C. A. Controlling the Direction of Rectification in a Molecular Diode. *Nat. Commun.* **2015**, *6*, 6324. https://doi.org/10.1038/ncomms7324.

(4) Zhou, P.; Fu, Y.; Wang, M.; Qiu, R.; Wang, Y.; Stoddart, J. F.; Wang, Y.; Chen, H. Robust Single-Supermolecule Switches Operating in Response to Two Different Noncovalent Interactions. *J. Am. Chem. Soc.* **2023**, *145* (34), 18800–18811. https://doi.org/10.1021/jacs.3c03282.

(5) Skipper, H.; Lawson, B.; Pan, X.; Degtiareva, V.; Kamenetska, M. Manipulating Quantum Interference between σ and π Orbitals in Single-Molecule Junctions via Chemical Substitution and Environmental Control. *ACS Nano* **2023**, *17* (16), 16107–16114. https://doi.org/10.1021/acsnano.3c04963.

(6) Datta, S. *Electronic Transport in Mesocopic Systems*; Cambridge University Press: Cambridge, UK, 1995.

(7) Tsuji, Y.; Movassagh, R.; Datta, S.; Hoffmann, R. Exponential Attenuation of Through-Bond Transmission in a Polyene: Theory and Potential Realizations. *ACS Nano* **2015**, *9* (11), 11109–11120. https://doi.org/10.1021/acsnano.5b04615.

(8) Perrin, M. L.; Perrin, M. L.; Eelkema, R.; Thijssen, J.; Grozema, F. C.; Van Der Zant, H.

S. J. Single-Molecule Functionality in Electronic Components Based on Orbital Resonances. *Phys. Chem. Chem. Phys.* **2020**, *22* (23), 12849–12866. https://doi.org/10.1039/D0CP01448F.

(9) Gunasekaran, S.; Greenwald, J. E.; Venkataraman, L. Visualizing Quantum Interference in Molecular Junctions. *Nano Lett.* **2020**, *20* (4), 2843–2848. https://doi.org/10.1021/acs.nanolett.0c00605.

(10) González-Herrero, H.; Mendieta-Moreno, J. I.; Edalatmanesh, S.; Santos, J.; Martín, N.; Écija, D.; de laTorre, B.; Jelinek, P.; González-Herrero, H.; Edalatmanesh, S.; et al. Atomic Scale Control and Visualization of Topological Quantum Phase Transition in π-Conjugated Polymers Driven by Their Length. *Adv. Mater.* **2021**, *33* (44), 2104495. https://doi.org/10.1002/ADMA.202104495.

(11) Li, L.; Low, J. Z.; Wilhelm, J.; Liao, G.; Gunasekaran, S.; Prindle, C. R.; Starr, R. L.; Golze, D.; Nuckolls, C.; Steigerwald, M. L.; et al. Highly Conducting Single-Molecule Topological Insulators Based on Mono- and Di-Radical Cations. *Nat. Chem.* **2022**, *14* (9), 1061–1067. https://doi.org/10.1038/s41557-022-00978-1.

(12) Naghibi, S.; Sangtarash, S.; Kumar, V. J.; Wu, J. Z.; Judd, M. M.; Qiao, X.; Gorenskaia, E.; Higgins, S. J.; Cox, N.; Nichols, R. J.; et al. Redox-Addressable Single-Molecule Junctions Incorporating a Persistent Organic Radical. *Angew. Chemie - Int. Ed.* **2022**, *61* (23), e202116985. https://doi.org/10.1002/anie.202116985.

(13) Li, L.; Louie, S.; Evans, A. M.; Meirzadeh, E.; Nuckolls, C. Topological Radical Pairs Produce Ultrahigh Conductance in Long Molecular Wires. *J. Am. Chem. Soc.* **2023**, *145* (4), 2492–2498. https://doi.org/10.1021/jacs.2c12059.

(14) Henson, J. D.; Reddel, R. R. Assaying and Investigating Alternative Lengthening of Telomeres Activity in Human Cells and Cancers. *FEBS Lett.* **2010**, *584* (17), 3800–3811. https://doi.org/10.1016/j.febslet.2010.06.009.

(15) Stuyver, T.; Zeng, T.; Tsuji, Y.; Geerlings, P.; De Proft, F. Diradical Character as a Guiding Principle for the Insightful Design of Molecular Nanowires with an Increasing Conductance with Length. *Nano Lett.* **2018**, *18* (11), 7298–7304. https://doi.org/10.1021/ACS.NANOLETT.8B03503/ASSET/IMAGES/LARGE/NL-2018-035039_0005.JPEG.

(16) Li, L.; Gunasekaran, S.; Wei, Y.; Nuckolls, C.; Venkataraman, L. Reversed Conductance Decay of 1D Topological Insulators by Tight-Binding Analysis. *J. Phys. Chem. Lett.* **2022**, *13* (41), 9703–9710. https://doi.org/10.1021/acs.jpclett.2c02812.

(17) Xu, B.; Tao, N. J. Measurement of Single-Molecule Resistance by Repeated Formation of Molecular Junctions. *Science (80-.).* **2003**, *301* (5637), 1221–1223. https://doi.org/10.1126/science.1087481.

(18) Venkataraman, L.; Klare, J. E.; Tam, I. W.; Nuckolls, C.; Hybertsen, M. S.; Steigerwald, M. L. Single-Molecule Circuits with Well-Defined Molecular Conductance. *Nano Lett.* **2006**, *6* (3), 458–462. https://doi.org/10.1021/nl052373+.

(19) McNeely, J.; Miller, N.; Pan, X.; Lawson, B.; Kamenetska, M. Angstrom-Scale Ruler Using Single Molecule Conductance Signatures. *J. Phys. Chem. C* **2020**, *124* (24), 13427–13433. https://doi.org/10.1021/acs.jpcc.0c02063.

(20) Hayashi, H.; Barker, J. E.; Cárdenas Valdivia, A.; Kishi, R.; Macmillan, S. N.; Gómez-García, C. J.; Miyauchi, H.; Nakamura, Y.; Nakano, M.; Kato, S. I.; et al. Monoradicals and Diradicals of Dibenzofluoreno[3,2- b]Fluorene Isomers: Mechanisms of Electronic Delocalization. *J. Am. Chem. Soc.* **2020**, *142* (48), 20444–20455.

https://doi.org/10.1021/jacs.0c09588.
(21) Dressler, J. J.; Cárdenas Valdivia, A.; Kishi, R.; Rudebusch, G. E.; Ventura, A. M.; Chastain, B. E.; Gómez-García, C. J.; Zakharov, L. N.; Nakano, M.; Casado, J.; et al. Diindenoanthracene Diradicaloids Enable Rational, Incremental Tuning of Their Singlet-Triplet Energy Gaps. *Chem* **2020**, *6* (6), 1353–1368. https://doi.org/10.1016/j.chempr.2020.02.010.
(22) Dressler, J. J.; Teraoka, M.; Espejo, G. L.; Kishi, R.; Takamuku, S.; Gómez-García, C. J.; Zakharov, L. N.; Nakano, M.; Casado, J.; Haley, M. M. Thiophene and Its Sulfur Inhibit Indenoindenodibenzothiophene Diradicals from Low-Energy Lying Thermal Triplets. *Nat. Chem.* **2018**, *10* (11), 1134–1140. https://doi.org/10.1038/s41557-018-0133-5.
(23) Choppella, S.; Paramasivam, G.; Sambasivam, S.; Ravva, M. K. Understanding the Stability of π-Conjugated Diradicaloid Organic Molecules. *J. Electron. Mater.* **2023**, *52* (3), 1681–1690. https://doi.org/10.1007/s11664-022-10082-2.
(24) Dressler, J. J.; Haley, M. M. Learning How to Fine-Tune Diradical Properties by Structure Refinement. *J. Phys. Org. Chem.* **2020**, *33* (July), 1–13. https://doi.org/10.1002/poc.4114.
(25) Frederickson, C. K.; Rose, B. D.; Haley, M. M. Explorations of the Indenofluorenes and Expanded Quinoidal Analogues. *Acc. Chem. Res.* **2017**, *50* (4), 977–987. https://doi.org/10.1021/acs.accounts.7b00004.
(26) Rudebusch, G. E.; Zafra, J. L.; Jorner, K.; Fukuda, K.; Marshall, J. L.; Arrechea-Marcos, I.; Espejo, G. L.; Ponce Ortiz, R.; Gómez-García, C. J.; Zakharov, L. N.; et al. Diindeno-Fusion of an Anthracene as a Design Strategy for Stable Organic Biradicals. *Nat. Chem.* **2016**, *8* (8), 753–759. https://doi.org/10.1038/nchem.2518.
(27) Reznikova, K.; Hsu, C.; Schosser, W. M.; Gallego, A.; Beltako, K.; Pauly, F.; Van Der Zant, H. S. J.; Mayor, M. Substitution Pattern Controlled Quantum Interference in [2.2]Paracyclophane-Based Single-Molecule Junctions. *J. Am. Chem. Soc.* **2021**, *143* (34), 13944–13951. https://doi.org/10.1021/JACS.1C06966/ASSET/IMAGES/LARGE/JA1C06966_0006.JPEG.
(28) Li, S.; Yu, H.; Li, J.; Angello, N.; Jira, E. R.; Li, B.; Burke, M. D.; Moore, J. S.; Schroeder, C. M. Transition between Nonresonant and Resonant Charge Transport in Molecular Junctions. *Nano Lett.* **2021**, *21* (19), 8340–8347. https://doi.org/10.1021/acs.nanolett.1c02915.
(29) Widawsky, J. R.; Kamenetska, M.; Klare, J.; Nuckolls, C.; Steigerwald, M. L.; Hybertsen, M. S.; Venkataraman, L. Measurement of Voltage-Dependent Electronic Transport across Amine-Linked Single-Molecular-Wire Junctions. *Nanotechnology* **2009**, *20* (43), 434009.
(30) Gu, J.; Wu, W.; Danovich, D.; Hoffmann, R.; Tsuji, Y.; Shaik, S. Valence Bond Theory Reveals Hidden Delocalized Diradical Character of Polyenes. *J. Am. Chem. Soc.* **2017**, *139* (27), 9302–9316. https://doi.org/10.1021/jacs.7b04410.
(31) Li, L.; Nuckolls, C.; Venkataraman, L. Designing Long and Highly Conducting Molecular Wires with Multiple Nontrivial Topological States. *J. Phys. Chem. Lett.* **2023**, *14*, 5141–5147. https://doi.org/10.1021/acs.jpclett.3c01081.
(32) Xu, W.; Leary, E.; Sangtarash, S.; Jirasek, M.; González, M. T.; Christensen, K. E.; Abellán Vicente, L.; Agraït, N.; Higgins, S. J.; Nichols, R. J.; et al. A Peierls Transition in Long Polymethine Molecular Wires: Evolution of Molecular Geometry and Single-Molecule Conductance. *J. Am. Chem. Soc.* **2021**, *143* (48), 20472–20481. https://doi.org/10.1021/jacs.1c10747.

(33) Gunasekaran, S.; Hernangómez-Pérez, D.; Davydenko, I.; Marder, S.; Evers, F.; Venkataraman, L. Near Length-Independent Conductance in Polymethine Molecular Wires. *Nano Lett.* **2018**, *18* (10), 6387–6391. https://doi.org/10.1021/ACS.NANOLETT.8B02743/SUPPL_FILE/NL8B02743_SI_001.PDF.
(34) Kiess, H. G. *Conjugated Conducting Polymers*; Springer-Verlag, 1992. https://doi.org/10.1007/978-3-642-46729-5.
(35) Castro Neto, A. H.; Guinea, F.; Peres, N. M. R.; Novoselov, K. S.; Geim, A. K. The Electronic Properties of Graphene. *Rev. Mod. Phys.* **2009**, *81* (1), 109–162. https://doi.org/10.1103/RevModPhys.81.109.
(36) Stauber, T.; Beltrán, J. I.; Schliemann, J. Tight-Binding Approach to Pentagraphene. *Sci. Rep.* **2016**, *6*, 4–11. https://doi.org/10.1038/srep22672.
(37) Verzijl, C. J. O.; Seldenthuis, J. S.; Thijssen, J. M. Applicability of the Wide-Band Limit in DFT-Based Molecular Transport Calculations. *J. Chem. Phys.* **2013**, *138* (9), 094102. https://doi.org/10.1063/1.4793259.
(38) Hernangómez-Pérez, D.; Gunasekaran, S.; Venkataraman, L.; Evers, F. Solitonics with Polyacetylenes. *ACS Appl. Mater. Interfaces* **2020**, *20* (4), 2615–2619. https://doi.org/10.1021/acs.nanolett.0c00136.
(39) Leary, E.; Limburg, B.; Alanazy, A.; Sangtarash, S.; Grace, I.; Swada, K.; Esdaile, L. J.; Noori, M.; González, M. T.; Rubio-Bollinger, G.; et al. Bias-Driven Conductance Increase with Length in Porphyrin Tapes. *J. Am. Chem. Soc.* **2018**, *140* (40), 12877–12883. https://doi.org/10.1021/jacs.8b06338.
(40) Deng, J.-R.; González, M. T.; Zhu, H.; Anderson, H. L.; Leary, E. Ballistic Conductance through Porphyrin Nanoribbons. *J. Am. Chem. Soc.* **2024**, *146* (6), 3651–3659. https://doi.org/10.1021/jacs.3c07734.
(41) Zang, Y.; Fu, T.; Zou, Q.; Ng, F.; Li, H.; Steigerwald, M. L.; Nuckolls, C.; Venkataraman, L. Cumulene Wires Display Increasing Conductance with Increasing Length. *Nano Lett.* **2020**, *20* (11), 8415–8419. https://doi.org/10.1021/acs.nanolett.0c03794.
(42) Xu, W.; Leary, E.; Hou, S.; Sangtarash, S.; González, M. T.; Rubio-Bollinger, G.; Wu, Q.; Sadeghi, H.; Tejerina, L.; Christensen, K. E.; et al. Unusual Length Dependence of the Conductance in Cumulene Molecular Wires. *Angew. Chemie - Int. Ed.* **2019**, *58* (25), 8378–8382. https://doi.org/10.1002/anie.201901228.
(43) Leary, E.; Roldán-Piñero, C.; Rico-Sánchez-Mateos, R.; Zotti, L. A. Antiaromatic Non-Alternant Heterocyclic Compounds as Molecular Wires. *J. Mater. Chem. C* **2024**, *12* (12), 4306–4315. https://doi.org/10.1039/d3tc04266a.
(44) Nieman, R.; Silva, N. J.; Aquino, A. J. A.; Haley, M. M.; Lischka, H. Interplay of Biradicaloid Character and Singlet/Triplet Energy Splitting for Cis-/ Trans-Diindenoacenes and Related Benzothiophene-Capped Oligomers as Revealed by Extended Multireference Calculations. *J. Org. Chem.* **2020**, *85* (5), 3664–3675. https://doi.org/10.1021/acs.joc.9b03308.
(45) Tsuji, Y.; Hoffmann, R.; Strange, M.; Solomon, G. C. Close Relation between Quantum Interference in Molecular Conductance and Diradical Existence. *Proc. Natl. Acad. Sci. U. S. A.* **2016**, *113* (4), E413–E419. https://doi.org/10.1073/PNAS.1518206113/-/DCSUPPLEMENTAL.
(46) Barker, J. E.; Dressler, J. J.; Cárdenas Valdivia, A.; Kishi, R.; Strand, E. T.; Zakharov, L. N.; Macmillan, S. N.; Gómez-García, C. J.; Nakano, M.; Casado, J.; et al. Molecule

Isomerism Modulates the Diradical Properties of Stable Singlet Diradicaloids. *J. Am. Chem. Soc.* **2020**, *142* (3), 1548–1555. https://doi.org/10.1021/jacs.9b11898.
(47) Kamenetska, M.; Koentopp, M.; Whalley, A. C.; Park, Y. S.; Steigerwald, M. L.; Nuckolls, C.; Hybertsen, M. S.; Venkataraman, L. Formation and Evolution of Single-Molecule Junctions. *Phys. Rev. Lett.* **2009**, *102* (12), 126803. https://doi.org/10.1103/PhysRevLett.102.126803.
(48) Lawson, B.; Zahl, P.; Hybertsen, M. S.; Kamenetska, M. Formation and Evolution of Metallocene Single-Molecule Circuits with Direct Gold-ΠLinks. *J. Am. Chem. Soc.* **2022**, *144* (14), 6504–6515. https://doi.org/10.1021/jacs.2c01322.